SAND2013-10763C

Large Eddy Simulation of Premixed Flame Flashback in a Turbulent Channel

Christopher Lietz, Malik Hassanaly, and Venkat Raman

Department of Aerospace Engineering and Engineering Mechanics,

The University of Texas at Austin, Austin, TX-78712

Hemanth Kolla and Jacqueline Chen

Sandia National Laboratory, Livermore, CA-94550

Andrea Gruber

SINTEF Energy Research, 7465 Trondheim, Norway

Corresponding author:

Christopher Lietz

Department of Aerospace Engineering and Engineering Mechanics

The University of Texas at Austin, Austin, TX-78712

Tel: +1 (262) 573-8293

E-mail: clietz@utexas.edu

- Count based on Method 2 (Latex based double-column formatted text)
- Number of words of text including figures and references = 6.33 pages $\times$ 900 = 5700.
- Total number of words **5700**
- Form of presentation: Oral.
- Colloquium topic: Turbulent Flames
- The authors agree to pay additional charges for color reproductions.

Large Eddy Simulation of Premixed Flame Flashback in a Turbulent Channel

Christopher Lietz[a], Malik Hassanaly[a], Venkat Raman[a], Hemanth Kolla[b], Jacqueline Chen[b], Andrea Gruber[c]

[a]*Dept. of Aerospace Engineering, The University of Texas at Austin, Austin, TX-78712*
[b]*Sandia National Laboratory, Livermore, CA*
[c]*SINTEF Energy Research, 7465 Trondheim, Norway*

Abstract

In the design of high-hydrogen content gas turbines for power generation, flashback of the turbulent flame by propagation through the low velocity boundary layers in the premixing region is an operationally dangerous event. Predictive models that could capture the onset of flashback would be indispensable in gas turbine design. For this purpose, modeling of the flashback process using the large eddy simulation (LES) approach is considered here. In particular, the goal is to understand the modeling requirements for predicting flashback in confined goemetries. The flow configuration considered is a turbulent channel flow, for which high-fidelity direct numerical simulation (DNS) data already exists. A suite of LES calculations with different model formulations and filterwidths is considered. It is shown that LES predicts certain statistical properties of the flame front reasonably well, but fails to capture the propagation velocity accurately. It is found that the flashback process is invariant to changes in the initial conditions and additional near-wall grid refinement but the LES filterwidth as well as the subfilter models are found to be important even when the turbulence is almost fully resolved.

From the computations, it is shown that for an LES model to predict flashback, sufficient resolution of the near-wall region, proper representation of the centerline acceleration caused by flame blockage, and appropriate modeling of the propagation of a wrinkled flame front near the center of the channel are considered the critical requirements.

Keywords: Large eddy simulation (LES), direct numerical simulations (DNS), boundary layer flashback

---

1. Introduction

In lean premixed combustion of fuels with high hydrogen content, preventing flame flashback is an important design constraint. The high reactivity of hydrogen combined with enhanced flammability limits (compared to natural gas) promotes flame propagation along low-speed boundary layers adjoining the combustion walls [1]. While this boundary layer flashback will be quenched by heat transfer to the walls, the combustor and premixing chamber walls may still sustain damage. Prior studies [2, 3] show that hydrogen flames are able to propagate three times closer to the wall before wall heat transfer quenches the flame. Since hydrogen-based power generation is a significant component of pre-combustion approaches for reducing carbon emissions, understanding and preventing flashback is a top priority in the design of such combustors.

Theoretical studies in laminar flames [4, 5, 6] have identified a critical near-wall velocity gradient necessary to arrest flashback. This relation correlates the burning velocity at the leading edge of the flame, the distance of this edge from the wall, and the velocity gradient at the wall. In general, a turbulent boundary layer exhibits a higher critical gradient as compared to a laminar boundary layer, which could be the result of a reduced distance to the wall or an increased burning velocity due to the core turbulent flow [7]. Computational studies mainly focused on laminar boundary layer flashback [4, 5, 6], with increasing complexity of the underlying flow description. Recently, Gruber et al. [8] conducted the first direct numerical simulation (DNS) of flame flashback in a three-dimensional channel flow using detailed chemical kinetics. The simulation indicates that density changes associated

with the flame strongly influence the propagation mechanism. Also, small reverse flow regions in front of the flame actively accelerate it.

In order to design robust combustors, tractable models that could predict flashback for a given combustor geometry and operating conditions would be indispensable. While many detailed computational models have been used to study other flashback modes, such as propagation through combustion induced vortex breakdown in swirl burners [9, 10], a similar focus on boundary layer flashback is missing. Due to the inherent three-dimensional and unsteady nature of flame flashback, the LES approach provides the best starting point for modeling. Since LES resolves only the large scales, and the flame/boundary layer interaction occurs exclusively at the small scales, subfilter models should be able to handle the impact of density changes on flame and fluid propagation. In the simulations of vortex breakdown based flashback [9, 10, 11], it has been found that existing models reproduce flashback with reasonable accuracy, but unphysical near-wall flame propagation could be introduced by the nature of the chemical source term closures used [10]. In these studies, flashback occurs primarily in the core of the flow, away from the walls, and subfilter closures based on the assumption of local equilibrium [12, 13] could be invoked without introducing appreciable errors. In boundary layer flashback, the balance of production and dissipation in the near wall region needs to be assessed in order to determine the accuracy of equilibrium-based subfilter models.

This discussion leads to the following question: What are the features of the flow that need to be reproduced for an LES-based model to predict flashback? To understand this question, we utilize *a posteriori* simulations

of a high-fidelity direct numerical simulation (DNS) configuration studied by Gruber et al [8] (We note that the DNS data used here is of higher resolution than the published data but otherwise unaltered. Details are provided in Sec. 2). Comparisons with DNS data have both advantages and disadvantages. On the positive side, DNS provides information about the entire flow field, which is ideal for testing individual models. On the downside, the Reynolds number of flow is relatively low, at only 3200. Further, the mesh is finer than the smallest turbulence length scale in order to resolve the flame front. In a confined geometry such as the channel studied here, these constraints impose a maximum and minimum resolution for the LES filterwidth. The filter size should be sufficiently large to obtain meaningful results from the loss of information due to filtering, and should be small enough that the boundary layer physics could be adequately represented.

With this background, the goal here is to assess the key physical characteristics that need to be represented in order to reproduce flashback using LES computations. A suite of LES computations is used to understand the key interactions between the flame and flow field. Statistical quantities describing the structure of the flame front are used to evaluate LES performance.

2. DNS flow configuration

Figure 1 shows a schematic of the flow configuration used in both the DNS and LES computations. The domain measures $0.06\,\mathrm{m} \times 0.012\,\mathrm{m} \times 0.036\,\mathrm{m}$ in the streamwise, wall-normal, and spanwise directions, respectively. In the DNS computation, a $2400 \times 480 \times 1440$ point computational grid is

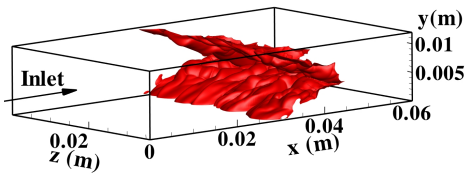

Figure 1: Channel schematic, with X aligned streamwise, Y wall normal, and Z spanwise. Instantaneous contour of $\widetilde{c} = 0.7$ for t = 7.880e-04 s, measured from the time of initialization.

used. The grid is uniform in all directions, giving a spacing of $\Delta_x = 2.5 \times 10^{-5}$ m. Premixed hydrogen-air mixture was fed through the inlet with a bulk velocity of 20 m/s leading to a Reynolds number of 3200. The equivalence ratio of the mixture was 0.55, and the inflow temperature was set at 750 K. The flow field was allowed to develop inside the channel for a finite time before the flame front was initialized at X = 0.045 m by superimposing a 1D laminar flame profile. The velocity field was adjusted to account for the change in density. Hydrogen combustion was simulated using a 9-species 19-step reaction mechanism [14]. The inflow to the DNS configuration was a temporally evolving turbulent velocity field extracted from an auxiliary inert DNS with a bulk velocity of 20 m/s. Although this configuration is slightly modified from that of [8], most other computational details remain the same.

Figure 2 shows instantaneous flame front contours at different times. As expected the flame progresses through the low velocity near-wall region, with the higher velocity near the channel centerline pushing the flame downstream. Not shown here, in the initial stages the flame is pushed downstream from the initialization point before flashback takes hold. The flame has a sinusoidal front near the walls (Fig. 1), indicating regions of positive curvature that

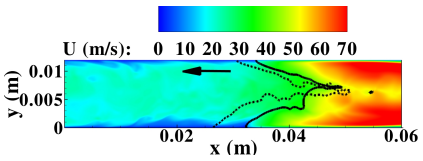

Figure 2: Instantaneous DNS contour of streamwise velocity component at t = 0.788 ms. The solid line represents the flame front isocontour based on C = 0.7 at that time instant, while the dashed line is the flame front at t = 1.44 ms. The arrow indicates the direction of flashback.

are accelerated as the flame propagates upstream. The DNS computation was run for a longer time but the data used in this work corresponds to the leading edge of the flame being displaced only by about 5 mm. However, flame propagation in this region is beyond the initial transient state and the upstream propagation velocity is roughly uniform.

The stream wise velocity component (Fig. 2) shows the acceleration of the flow behind the flame front. The flame front acts as a blockage for the flow which diverts the near-wall fluid toward the centerline causing an acceleration before reaching the flame. The gas expansion causes a second acceleration that make the velocity reach values close to 70 m/s. Figure 2 also shows the flame front at the earliest and latest time instances that encompass the entirety of the DNS data used in this work. Note that in this duration, the flame front motion is almost uniform allowing for temporal averaging in collecting statistics.

3. LES computations

The LES approach uses a grid-based filtering technique. The flame evolution is described using a flamelet approach, where a transport equation for the Favre-filtered progress variable is solved along with the filtered continuity and momentum equations. A low-Mach number technique based on a pressure-projection algorithm is used [15, 16]. The filtered transport equation for progress variable is given by

$$\frac{\partial \overline{\rho}\widetilde{c}}{\partial t} + \frac{\partial \overline{\rho}\widetilde{u_i}\widetilde{c}}{\partial x_i} = \frac{\partial}{\partial x_i}\alpha(\widetilde{c},\Delta)\overline{\rho}D\frac{\partial \widetilde{c}}{\partial x_i} + \frac{\partial}{\partial x_i}\overline{\rho}\left(\widetilde{u_i c} - \widetilde{u_i}\widetilde{c}\right) + \widetilde{\dot{\omega}}, \qquad (1)$$

where α is a model for the correlation between the diffusivity and the scalar gradient, Δ is the LES filterwidth and $\widetilde{\dot{\omega}}$ is the chemical source term. The second term on the right hand side is the subfilter scalar flux term. In general, there are many different models available for closing these terms [17, 18, 19, 20, 21]. In order to ensure that our conclusions are not biased by the models used, three different models are tested here. All the models used here ignore differential diffusion effects. An analysis of the equivalence ratio variations across the flame front in the DNS showed that the maximum change was small compared to the mean equivalence ratio. The details of the models are as follows:

1. Direct flamelet model (DF). Here, the 1-D laminar premixed solution is mapped to progress variable space, and no convolution rules are used to transform the raw progress variable to a filtered value. This model represents the crudest approximation of the flame front. Here α is set to 1, and the subfilter flux is modeled using gradient-diffusion hypothesis.

2. Algebraic flame surface density model (AFSD). Here, the first and third terms together are modeled using the flame surface density.

$$\frac{\partial}{\partial x_i}\alpha(\widetilde{c},\Delta)\overline{\rho}D\frac{\partial\widetilde{c}}{\partial x_i}+\widetilde{\dot{\omega}}=\rho_u S_l\Sigma, \tag{2}$$

where ρ_u, S_l and Σ are the unburnt density, laminar burning velocity, and flame surface density (FSD). The FSD is closed using an algebraic model [20] that relates the subfilter variance of progress variable to the FSD.

$$\Sigma=4\beta\frac{\overline{c}(1-\overline{c})}{\Delta}, \tag{3}$$

with β being a tunable coefficient and Δ the LES filterwidth. Here, the value of β is chosen such that certain properties of the DNS are reproduced. This is further discussed in Sec. 4.2. The subfilter flux term is prescribed using a gradient diffusion hypothesis.

3. Filtered tabulated chemistry for LES (FTACLES) [19]. Here, the 1D laminar flame solution is filtered using an explicit Gaussian filter with the specified LES filterwidth. The resulting filtered progress variable is used as the mapping variable. In this approach, α is specifically constructed from the flame solution. As described by [22], the three terms on the right hand side of Eq. 1 can be directly obtained from this filtering procedure. Figure 3 shows the different terms plotted as a function of the filtered progress variable. Note that for the filter width for $8\Delta_x$, the subfilter terms are negligible since the flame wrinkling is almost fully resolved. In this sense, the FTACLES approach will be similar to the DF method here. For larger filter widths, the differences

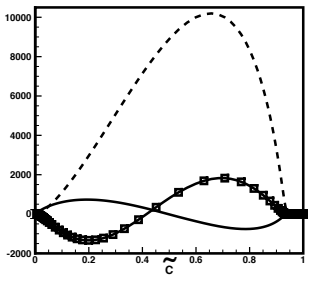

Figure 3: Filtered source terms obtained from the FTACLES procedure for filter width $8\Delta_x$: $\frac{\partial}{\partial x_i}\alpha(\widetilde{c},\Delta)\overline{\rho}D\frac{\partial\widetilde{c}}{\partial x_i}$ (solid line), $-\nabla\cdot\overline{\rho}\left(\widetilde{u_i c}-\widetilde{u}_i\widetilde{c}\right)$ (solid line with symbols), and $\overline{\rho}\widetilde{\dot{\omega}}$ (dashed line). Y-axis has units of kg/m^{3}s.

will be large.

Note that all three models essentially replace the finite thickness flame front with a thin flame assumption. Since the LES filter width is sufficiently small, flame wrinkling is expected to be fully resolved. As pointed out by [23], with increasing computational power, this regime where turbulence is well resolved has become the norm. Consequently, representing laminar flame propagation accurately with minimal computational cost becomes the critical step.

The flow equations contain unresolved stress terms, which are closed here using a dynamic Smagorinksy model. The LES equations are solved using a second-order accurate time-stepping scheme [24, 25]. The convection terms in the momentum equations are discretized using an energy conserving second order scheme, while the scalar convection terms were solved using the QUICK scheme [26]. The simulations were carried out using MPI-based domain decomposition.

The LES calculations used the same inflow conditions as the DNS calcula-

tion, except that the inflow planes were interpolated to the coarser LES grid. Each LES computation was run without a flame until any initial transient was removed. The flame is initialized at $X = 0.03\,\mathrm{m}$ in the LES calculation. Note that in the DNS, the flame is initialized at $X = 0.045\,\mathrm{m}$. This difference was necessary to ensure that strong density jumps from the trailing edge of the flame were not present close to the exit. The velocity was adjusted for the density jump across the initially flat flame, and the simulations continued from that point.

4. Results and discussion

Two different groups of LES calculations are carried out. First, the effect of models is tested using the three models described above. Second, the effect of filter width is discussed. A third set of calculations where the LES is initialized using different initial conditions for the flow field was also carried out. For these calculations, an LES filterwidth of $16\Delta_x$ along with the FTACLES model was used. There was no appreciable change in the flame front propagation for the different cases in this set. This implies that flame front propagation is the accumulated interaction with multiple eddies over resolved-scale time scale, and that variability in initial conditions are washed out by the short length-scale associated with eddies that affect the flame front.

Before discussing the two sets of calculations, the baseline case is presented in detail to motivate the key parameters targeted in the flashback computations.

4.1. Baseline LES computation of flashback

The baseline case is based on the FTACLES model with $\Delta = 8\Delta_x$. Figure 4 shows the LES-based isosurface of $\widetilde{c} = 0.7$ at the earliest and latest time for which corresponding DNS data is available. Two things to note here. First, although the LES flame was initialized upstream of the DNS flame, at these time instances, both DNS and LES flame fronts are fairly close in streamwise location. Second, at the latest time, the flame front has a similar structure to that found in the DNS computation (Fig. 2). But, at the earlier time, the flame front is less stretched and remains closer to the flat initial condition. This shows that the LES and DNS have different evolution times before a quasi-steady flame front propagation could be reached. At a more fundamental level, this shows that LES predicts the growth in flame wrinkling and flame stretch at a much slower rate as compared to the DNS computation. In both the LES and the DNS, the flow is diverted away from the walls by the flame-induced blockage, which causes an acceleration of the flow along the center. Gas expansion in the post-flame region further increases the flow rate. However, in the LES calculation at earlier time, the lack of a v-shaped flame prevents the centerline acceleration. Consequently, the post-flame velocities are much lower than that for DNS and are essentially the density-scaled turbulent channel flow velocities. At later times as the flame front becomes similar to the DNS, the post-flame velocities are of the same order as DNS (not shown here).

Figure 5 shows the three-dimensional isosurface of progress variable at a time comparable to that of the DNS in Fig. 1. It is seen that the DNS surface exhibits a wide range of scales (as expected) with smooth variations on

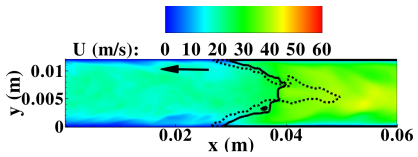

Figure 4: Instantaneous LES contour of streamwise velocity component at t = 0.8 ms. The solid line represents the flame front isocontour based on C = 0.7 at that time instant, while the dashed line is the flame front at t = 1.4 ms. The arrow indicates the direction of flashback.

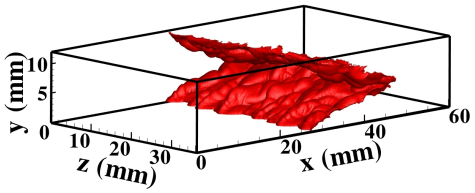

Figure 5: Instantaneous isocontour of $\tilde{c} = 0.7$ and isocontours of streamwise vorticity for 7500 1/s.

the surface interspersed with short-lengthscale fluctuations in the streamwise location of the flame front. In addition, the positive curvature regions near the wall that tend to accelerate the flame are more pronounced with deeper troughs along the streamwise direction. Although the LES flame surface exhibits similar troughs, the depth of these features is considerably smaller. As a consequence, the spanwise variation in the flame front location in the near wall region is smaller compared to the DNS case.

To further understand the LES results, the evolution of the distance between the leading and trailing edges of the flame is studied. For the purpose of this discussion, the leading edge is the first point along the x-axis in a single z-plane that contains a non-zero progress variable, while the trailing edge

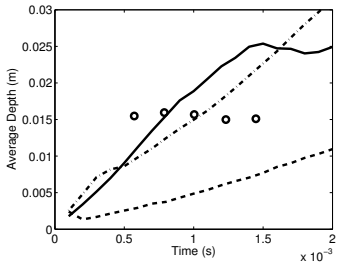

Figure 6: Plot of spanwise averaged depth parameter as a function of time for DNS (circles) and LES with FTACLES (solid line), FSD with $\beta = 0.2$ (dash-dotted line), and FSD with $\beta = 0.66$ (dashed line) at $\Delta/\Delta_x = 8$.

is the last grid point in the x-direction that contains a zero progress variable. This quantity, termed flame depth here, incorporates the cumulative effect of the core velocity on the propagation characteristics. Note that in the boundary layers where the flow field is nearly laminar, propagation is mainly at the laminar flame speed (adjusted for quenching effects), while in the core flow, turbulent flame wrinkling will lead to turbulent-velocity based propagation. In the extreme case of the depth being zero, the difference between the core velocity and the turbulent propagation speed matches the difference between the laminar burning velocity and the boundary layer mean velocity.

Figure 6 shows the spanwise-averaged depth as a function of time. It is seen for the baseline case that this quantity increases with time but ultimately reaches a slowly varying stage after 1.4 ms. The depth in the DNS is steady in this time interval at roughly 0.015 m. The increase in LES is expected as the flame is wrinkled from its initial flat condition. But the continued growth indicates that a) the trailing edge of the flame is not able to propagate strongly against the high velocity near the centerline, and b) the streamwise

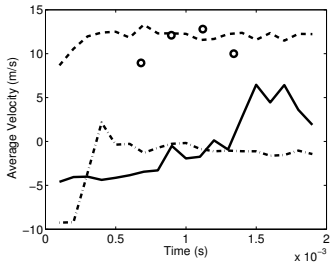

Figure 7: Plot of spanwise averaged velocity as a function of time for DNS (circles) and LES with FTACLES (solid line), FSD with $\beta = 0.2$ (dash-dotted line), and FSD with $\beta = 0.66$ (dashed line) at $\Delta/\Delta_x = 8$.

velocity in the near-wall region ahead of the leading edge of flame is weaker than in DNS leading to faster flame propagation, relative to the center of the flame. Figure 7 shows the propagation velocity averaged based on the top and bottom leading edges and the trailing edge of the flame. It can be seen that initially the flame is convected downstream (negative velocity) before flashback takes hold. But even then, the propagation velocity is much lower than the DNS velocity. This explains the observation made earlier that both flame fronts are at similar locations for the time-intervals considered even when starting from different initial locations.

A related quantity of interest is the fluctuation of the flame front location in the streamwise direction about the spanwise-averaged flame front location. Figure 8 shows the PDF of the flame location in both DNS and LES computations. It is seen that the LES-based PDF roughly matches the near-Gaussian DNS-based PDF. However, the probability of large fluctuations is marginally lower than the DNS probability. Overall, the baseline LES is able to capture most of the details of the flame front albeit with different initialization

locations.

4.2. Effect of flame model on propagation

To understand the role of the model in predicting the parameters of flashback defined in the previous section, the three different models described in Sec. 3 were used with LES filterwidth of $8\Delta_x$. The DF model produced results similar to the FTACLES approach. This is expected, given that the filter width is small compared to the DNS mesh size. Hence, the diffusivity and subfilter scalar flux closures remain small compared to the chemical source term (see Fig. 3). The results from the the DF model are not presented here due to the similarity with FTACLES, but serve to illustrate the impact of other subfilter models on flame evolution.

The AFSD model, on the other hand, shows interesting behavior. The coefficient β is roughly 0.75 from literature for $\Delta/\Delta_x = 8$ [20]. However, this value was found to cause unphysical motion of the flame front, with the flame propagating through the center of the channel. A sequence of AFSD model simulations were carried out to find the optimum value for the coefficient. It was found that if $\beta = 0.2$, then the depth parameter from the simulations were close the DNS data at 1 ms (Fig. 6). However, the average velocity of the flame was found to be negative for this simulation, where the leading edge was slowly propagating upstream while the trailing edge was being convected out more rapidly. When $\beta = 0.66$, the right propagation velocity could be obtained at 1 ms but the depth was far less than in the DNS. Figure 8 also shows that even when the depth parameter is reasonably predicted, the AFSD model has limited fluctuations about the mean flame surface.

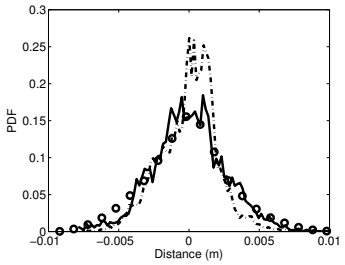

Figure 8: PDF of distance from the $\widetilde{c} = 0.7$ isocontour for DNS (circles) and LES with FTACLES (solid line) and FSD with $\beta = 0.2$ (dash-dotted line) at $\Delta/\Delta_x = 8$.

Figure 9 shows the velocity obtained from the FSD model superimposed with flame front isocontours from the two calculations with different β values. It can be seen that even when the depth is correctly predicted, the flame shape is very different from the flamelet-based computations. There is a thin layer near the wall where the flame flashes back, but a parabolic flame front is visible in the rest of the domain. With an increase in β, the propagation speed increases and the thin near-wall flam region vanishes. In either case, the shape of the flame does not lead to significant centerline acceleration of the flow, and the post-flame velocities are small compared to the fully-developed FTACLES flame front.

While the deficiencies of the algebraic model are well noted [10, 27], the simple nature of the source term also provides insight into the flame propagation. When the coefficient is low, it reduces the source term for the progress variable. However, the source term does not distinguish between regions of high or low scalar gradient. Consequently, the leading edge and trailing edge propagate at the same speed. The reduced coefficient only ensures that the fluid near the centerline is able to push out flame, while the leading of the

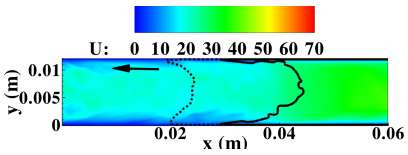

Figure 9: Instantaneous LES contour of streamwise velocity component at t = 1 ms for FSD model with $\beta = 0.2$. The solid line represents the flame front isocontour based on C = 0.7 for $\beta = 0.2$ while the dashed line is $\beta = 0.66$, both at t = 1 ms. The The arrow indicates the direction of flashback.

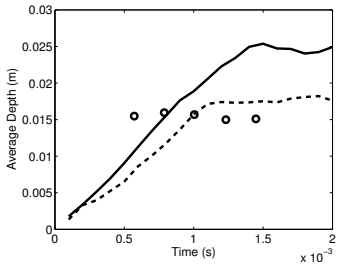

Figure 10: Plot of spanwise averaged depth parameter as a function of time for DNS (circles) and LES with FTACLES at $\Delta/\Delta_x = 8$ (solid line) and $\Delta/\Delta_x = 16$ (dashed line).

flame slowly creeps up the channel. When the coefficient is large, the flame near the centerline propagates faster, leading a reduction in depth. This is consistent with the observation that as β increases, the curvature of the flame switches and flashback occurs along the centerline.

4.3. Effect of LES grid on propagation

The main variation in grid was to study $\Delta = 8\Delta_x$ and $\Delta = 16\Delta_x$ with the FTACLES model. In addition, the computational grid associated with each width was refined in the wall-normal direction to add twice the number of points in the low-velocity region. Grid clustering did not change the

propagation speed nor the depth parameter as compared to the uniform mesh case for both filterwidths. This was surprising as better near-wall resolution should be expected to better represent the flashback process. This suggests that a minimum resolution is needed to reproduce flashback but additional resolution does not necessarily introduce any new physics capable of altering the flame dynamics. However, the change of filterwidth from $8\Delta_x$ to $16\Delta_x$ had a large effect. Figure 10 shows the evolution of the depth parameter for the two filterwidths and it can be seen that the coarser mesh reproduces the DNS depth accurately, while the finer mesh overpredicts the depth parameter. It should be noted that the agreement with DNS data for $\Delta = 16\Delta_x$ could very well be fortuitous but the decrease in depth is interesting. We postulate that this change is related to coarser resolution of the turbulence structure in the core of the flow. This in turn allows the trailing edge of the flame to propagate faster due to reduced centerline velocities. Mesh coarsening also increases the average propagation velocity, although this difference is minimized at later times. A larger filter $\Delta = 24\Delta_x$ was not able to reproduce the expected V-shape of the flame. Instead, the flame flashed back with a flat shape, highlighting the importance of the near-wall resolution. Overall, the propagation velocity still eludes the LES computations.

5. Conclusions

A suite of LES computations was used to understand the modeling of boundary layer flashback in relatively low Reynolds number but turbulent channel flow. The LES filterwidths were comparable to the smallest turbulence length scales, which would imply that the momentum description is

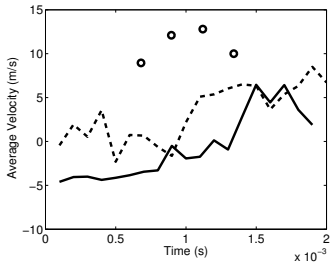

Figure 11: Plot of spanwise averaged velocity as a function of time for DNS (circles) and LES with FTACLES at $\Delta/\Delta_x = 8$ (solid line) and $\Delta/\Delta_x = 16$ (dashed line).

reasonably accurate in the LES calculations. The flame, on the other hand, was approximated as a thin front using different models. In this sense, the computations were designed to test the interaction of this thin-flame assumption with the near-fully resolved flow field. The computations found certain intriguing features. The baseline case at filterwidth of 8 produced a flame front that is comparable in statistics to that in the DNS. Using quantities such as the depth parameter and the PDF of front fluctuations, it was found that the LES computations are very accurate in predicting the structure of the turbulent flame front. However, there was a large discrepancy in the propagation velocity of the flame front. In other words, a slowly moving LES flame front was able to produce the structures of a faster moving DNS front. The flamelet-based models produced lesser variability to simulation conditions, including the choice of other subfilter models. This is expected, given that the chemical source term is the predominant quantity in the progress variable transport equation as it can be seen in Figure 3. On the other hand, the AFSD model produced unexpected results, with lower reaction rates reproducing the DNS depth and the higher velocities reproducing the DNS

propagation velocity. Further, the flame depth decreases with increasing filterwidth, and the flashback velocity increases with filterwidth.

These observations indicate that although the flame is well represented by the flamelet model, the differences in propagation mechanisms between the near-wall region and the center of the channel are not captured well. There is no wrinkling model used in this work, since the flow conditions would indicate that all the wrinkling is fully resolved. It appears that this assumption is not fully valid in the *a posteriori* simulation, where numerical errors at the smallest resolved scales tend to alter flame physics [28]. The AFSD model results illustrate this point, where higher reaction rates tend to make the trailing edge of the flame located in the center of the channel to flashback faster, while lower values cause the trailing edge to be progressively swept out.

Even for the lowest resolution grids, flashback was still predicted, indicating that flame propagation through the boundary layers could be captured with minimal resolution. Interestingly, additional variations on these basic computations did not produce any changes to the flow. For instance, adding more points to the near-wall region did not change the depth or the velocity of propagation. Also, starting the calculation from different initial conditions led to almost no perceptible difference in these characteristics of the flame.

Based on these results, the requirements to capture the flashback process could be divided into three parts. First, there should be sufficient resolution near the wall to represent the actual V-shape of the flame, and at least approximately, the transition to a laminar flow. Combined with the density change across the flame, this creates a blockage to divert the flow towards

the center. Second, the blockage-created centerline acceleration in the core of the channel is necessary to maintain the V-shape of the flame. Third, the combustion model should ensure that the core is not pushed downstream with the flow. In other words, the transition from a fully laminar to, possibly unresolved, wrinkled flame needs to be captured. However, the requirements for obtaining the correct propagation velocity seem to rely on the details of the model. For instance, the modulation of the small-scale turbulence by the density change across the flame front, as well as the impact of near-wall streaks need to be included in the closure model, in order to accurately represent the specific features of a flashback in a rectangular channel.

6. Acknowledgements

CL, MH, and VR were supported by a DOE-NETL grant DE-FE0007107. This research used resources of the Oak Ridge Leadership Computing Facility at the Oak Ridge National Laboratory, which is supported by the Office of Science of the U.S. Department of Energy under Contract No. DE-AC05-00OR22725 and the National Energy Research Scientific Computing Center, which is supported by the Office of Science of the U.S. Department of Energy under Contract No. DE-AC02-05CH11231.

References

[1] J. Fritz, M. Kroner, T. Sattelmayer, Journal of Engineering for Gas Turbines and Power-Transactions of the ASME 126 (2004) 276–283.

[2] F. Dabireau, B. Cuenot, O. Vermorel, T. Poinsot, Combustion and Flame 135 (2003) 123–133.

[3] A. Gruber, R. Sankaran, E. Hawkes, J. H. Chen, Journal of Fluid Mechanics 658 (2010) 5–32.

[4] G. Lewis, Proceedings of the Combustion Institute 14 (1973).

[5] V. Kurdyumov, E. Fernandez-Tarrazo, J. Truffaut, J. Quinard, A. Wangher, G. Searby, in: Proceedings of the Combustion Institute, volume 31, pp. 1275–1282.

[6] V. Kurdyumov, E. Fernandez-Tarrazo, A. Linan, in: Proceedings of the Combustion Institute, volume 28, pp. 1883–1889.

[7] C. Eichler, T. Sattelmayer, Journal of Engineering for Gas Turbines and Power 133 (2011).

[8] A. Gruber, J. H. Chen, D. Valiev, C. K. Law, Journal of Fluid Mechanics 709 (2012) 516–542.

[9] Y. Sommerer, D. Galley, T. Poinsot, S. Ducruix, F. Lacas, D. Veynante, Journal of Turbulence 5 (2004).

[10] E. Tangermann, M. Pfitzner, Journal of Turbulence 10 (2009) 1–21.

[11] D. Thibaut, S. Candel, Combustion and Flame 113 (1998) 53–65.

[12] P. Moin, K. Squires, W. Cabot, S. Lee, Physics of Fluids A 3 (1991) 2746–2757.

[13] J. Smagorinsky, Monthly Weather Review 91 (1963) 99–164.

[14] J. Li, Z. Zhao, A. Kazakov, F. Dryer, International Journal of Chemical Kinetics 36 (2004) 566–575.

[15] C. D. Pierce, P. Moin, Journal of Fluid Mechanics 504 (2004) 73–97.

[16] K. Akselvoll, P. Moin, Journal of Fluid Mechanics 315 (1996) 387–411.

[17] F. Colin, F. Ducros, D. Veynante, T. Poinsot, Physics of Fluids 12 (2000) 1843–1863.

[18] F. Hernandez-Perez, F. Yuen, C. Groth, O. Gulder, in: Proceedings of the Combustion Institute, volume 33, pp. 1365–1371.

[19] P. Auzillon, R. Vicquelin, O. Gicquel, N. Darabiha, D. Veynante, B. Fiorina, in: 48th AIAA Aerospace Sciences Meeting.

[20] M. Boger, D. Veynante, H. Boughanem, A. Trouve, Twenty-Seventh Symposium (International) on Combustion 27 (1998) 917–925.

[21] G. Tabor, H. Weller, Flow, Turbulence and Combustion 72 (2004) 1–28.

[22] P. Auzillon, B. Fiorina, R. Vicquelin, N. Darabiha, O. Gicquel, D. Veynante, in: Proceedings of the Combustion Institute, volume 33, pp. 1331–1338.

[23] B. Fiorina, O. Gicquel, L. Vervisch, S. Carpentier, N. Darabiha, Combustion and Flame 140 (2005) 147–160.

[24] C. D. Pierce, Progress-variable approach for large-eddy simulation of turbulence combustion, Ph.D. thesis, Stanford University, 2001.

[25] P. E. Desjardin, S. H. Frankel, Physics of Fluids 10 (1998) 2298–2314.

[26] B. P. Leonard, Computational Methods in Applied Mechanics 19 (1979) 59–98.

[27] E. Hawkes, S. Cant, Proceedings of Combustion Institute 28 (2000) 51–58.

[28] C. Kaul, V. Raman, E. Richardson, J. H. Chen, in: Proceedings of the Combustion Institute, volume 34, pp. 1289–1297.

List of Figures